

# Evolution of order and chaos across a first-order quantum phase transition

A. Leviatan and M. Macek

*Racah Institute of Physics, The Hebrew University, Jerusalem 91904, Israel*

(Dated: April 21, 2019)

We study the evolution of the dynamics across a generic first order quantum phase transition in an interacting boson model of nuclei. The dynamics inside the phase coexistence region exhibits a very simple pattern. A classical analysis reveals a robustly regular dynamics confined to the deformed region and well separated from a chaotic dynamics ascribed to the spherical region. A quantum analysis discloses regular bands of states in the deformed region, which persist to energies well above the phase-separating barrier, in the face of a complicated environment. The impact of kinetic collective rotational terms on this intricate interplay of order and chaos is investigated.

PACS numbers: 21.60.Fw, 05.45.Mt, 05.30.Rt, 21.10.Re

Quantum phase transitions (QPTs) are qualitative changes in the properties of a physical system induced by a variation of parameters  $\lambda$  in the quantum Hamiltonian  $\hat{H}(\lambda)$  [1, 2]. Such ground-state transformations have received considerable attention in recent years and have found a variety of applications in many areas of physics and chemistry [3]. The competing interactions in the Hamiltonian that drive these transitions, can affect dramatically the nature of the dynamics and, in some cases, lead to the emergence of quantum chaos. This effect has been observed in quantum optics models of  $N$  two-level atoms interacting with a single-mode radiation field [4], where the onset of chaos is triggered by continuous QPTs. In this case, the underlying mean-field (Landau) potential  $V(\lambda)$  has a single minimum which evolves continuously into another minimum. The situation is more complex for discontinuous (first-order) QPTs. Here  $V(\lambda)$  develops multiple minima that coexist in a range of  $\lambda$  values and cross at the critical point,  $\lambda = \lambda_c$ . Understanding the nature of the underlying dynamics in such circumstances is a primary goal of the present Letter.

The interest in first-order QPTs stems from their key role in phase-coexistence phenomena at zero temperature. In condensed matter physics, it has been recently recognized that, for clean samples, the nature of the QPT becomes discontinuous as the critical-point is approached. Examples are offered by the metal-insulator Mott transition [5], itinerant magnets [6], heavy-fermion superconductors [7], and quantum Hall bilayers [8]. First-order QPTs are relevant to shape-coexistence in mesoscopic systems, such as atomic nuclei [9], and to optimization problems in quantum computing [10].

Hamiltonians describing first-order QPTs are often non-integrable, hence their dynamics is mixed. They form a subclass among the family of generic Hamiltonians with a mixed phase space, in which regular and chaotic motion coexist. In the present Letter, we wish to illuminate, in a transparent manner, those aspects of this mixed dynamics which reflect the first-order transition. For that purpose, we employ an interacting boson model which describes such QPTs between spheri-

cal and axially-deformed nuclei. Our main results are that, (i) in spite of the abrupt structural changes taking place across a first-order QPT, the dynamics in the coexistence region exhibits a very simple pattern. A robustly regular dynamics is confined to the deformed region, and is well separated from the chaotic dynamics ascribed to the spherical region. (ii) The deviations from this marked separation is largely due to kinetic collective rotational terms in the Hamiltonian. This simple pattern of mixed dynamics was initially observed at the critical point,  $\lambda = \lambda_c$  [11]. Here we show it to be a hallmark of the whole coexistence region. Simply divided phase spaces were encountered in billiard systems [12, 13], which are generated by the free motion of a point particle inside a closed domain whose geometry governs the amount of chaoticity. Here, in contrast, we consider many-body interacting systems undergoing QPTs, where the onset of chaos is governed by a change of coupling constants in the Hamiltonian.

The interacting boson model (IBM) [14] describes quadrupole collective states in nuclei in terms of a system of  $N$  monopole ( $s$ ) and quadrupole ( $d$ ) bosons, representing valence nucleon pairs. The Hamiltonian conserves the total boson number  $N$  and angular momentum  $L$ . Its geometric visualization is obtained by a potential surface,  $V(\beta, \gamma) = \langle \beta, \gamma; N | \hat{H} | \beta, \gamma; N \rangle$ , defined by the expectation value of the Hamiltonian in the intrinsic condensate state  $|\beta, \gamma; N\rangle = (N!)^{-1/2} [\Gamma_c^\dagger(\beta, \gamma)]^N |0\rangle$ , where  $\Gamma_c^\dagger(\beta, \gamma) = \frac{1}{\sqrt{2}}[\beta \cos \gamma d_0^\dagger + \beta \sin \gamma \frac{1}{\sqrt{2}}(d_2^\dagger + d_{-2}^\dagger) + \sqrt{2 - \beta^2} s^\dagger]$ . Here  $(\beta, \gamma)$  are quadrupole shape parameters whose values  $(\beta_{\text{eq}}, \gamma_{\text{eq}})$  at the global minimum of  $V(\beta, \gamma)$  define the equilibrium shape for a given Hamiltonian. QPTs between such stable shapes have been studied extensively in the IBM framework [15–17] and are manifested empirically in nuclei [9]. Their nature is dictated by the topology of  $V(\beta, \gamma)$ , which serves as a Landau potential. For that reason, in studying such QPTs, it is convenient to resolve the Hamiltonian into two parts [18],

$$\hat{H} = \hat{H}_{\text{int}} + \hat{H}_{\text{col}} . \quad (1)$$

The intrinsic part ( $\hat{H}_{\text{int}}$ ) determines the potential surface

$V(\beta, \gamma)$ , while the collective part ( $\hat{H}_{\text{col}}$ ) is composed of kinetic terms which do not affect the shape of  $V(\beta, \gamma)$ .

Focusing on first-order QPTs between stable spherical ( $\beta_{\text{eq}} = 0$ ) and prolate-deformed ( $\beta_{\text{eq}} > 0$ ,  $\gamma_{\text{eq}} = 0$ ) shapes, the intrinsic Hamiltonian reads

$$\hat{H}_{\text{int}}^I(\rho)/\hbar_2 = 2(1 - \rho^2 \beta_0^2) \hat{n}_d(\hat{n}_d - 1) + \beta_0^2 R_{2\mu}^\dagger \cdot \tilde{R}_{2\mu}, \quad (2a)$$

$$\hat{H}_{\text{int}}^{II}(\xi)/\hbar_2 = \xi P_0^\dagger P_0 + P_2^\dagger \cdot \tilde{P}_2, \quad (2b)$$

where  $\hat{n}_d = \sum_\mu d_\mu^\dagger d_\mu$  is the  $d$ -boson number operator,  $R_{2\mu}^\dagger(\rho) = \sqrt{2} s^\dagger d_\mu^\dagger + \rho \sqrt{7} (d^\dagger d^\dagger)_\mu^{(2)}$ ,  $P_0^\dagger(\beta_0) = d^\dagger \cdot d^\dagger - \beta_0^2 (s^\dagger)^2$  and  $P_{2\mu}^\dagger(\beta_0) = \sqrt{2} \beta_0 s^\dagger d_\mu^\dagger + \sqrt{7} (d^\dagger d^\dagger)_\mu^{(2)}$ . Here  $\tilde{R}_{2\mu} = (-1)^\mu R_{2, -\mu}$ ,  $\tilde{P}_{2\mu} = (-1)^\mu P_{2, -\mu}$  and the dot implies a scalar product. Scaling by  $\hbar_2 \equiv h_2/N(N-1)$  is used throughout, to facilitate the comparison with the classical limit. The control parameters that drive the QPT are  $\rho$  and  $\xi$ , with  $0 \leq \rho \leq \beta_0^{-1}$  and  $\xi \geq 0$ , while  $\beta_0$  is a constant. For the indicated ranges, the intrinsic Hamiltonians in the spherical [ $\hat{H}_{\text{int}}^I(\rho)$ ] and deformed [ $\hat{H}_{\text{int}}^{II}(\xi)$ ] phases have the intrinsic states  $|\beta_{\text{eq}}, \gamma_{\text{eq}}; N\rangle$  with, respectively,  $\beta_{\text{eq}} = 0$  and  $[\beta_{\text{eq}} > 0, \gamma_{\text{eq}} = 0]$ , as zero-energy ground states. For large  $N$ , the normal modes of  $\hat{H}_{\text{int}}^I(\rho)$  [ $\hat{H}_{\text{int}}^{II}(\xi)$ ] involve quadrupole [both  $\beta$  and  $\gamma$ ] vibrations about the spherical [deformed] global minimum, with frequency  $\epsilon = 2\hbar_2 N \beta_0^2 [\epsilon_\beta = 2\hbar_2 N \beta_0^2 (2\xi + 1), \epsilon_\gamma = 18\hbar_2 N \beta_0^2 (1 + \beta_0^2)^{-1}]$ . The two Hamiltonians coincide at the critical point  $\rho_c = \beta_0^{-1}$  and  $\xi_c = 0$ :  $\hat{H}_{\text{int}}^I(\rho_c) = \hat{H}_{\text{int}}^{II}(\xi_c)$ , being equal to the Hamiltonian studied in [11].

The classical limit of the IBM is obtained through the use of coherent states and taking  $N \rightarrow \infty$ , with  $1/N$  playing the role of  $\hbar$  [19]. Number conservation ensures that phase space is 10-dimensional and can be phrased in terms of two shape (deformation) variables, three orientation (Euler) angles and their conjugate momenta. The classical Hamiltonian obtained involves complicated expressions (including square roots) of these variables. Setting all momenta to zero, yields the classical potential which is identical to  $V(\beta, \gamma)$  mentioned above. Chaotic properties of the IBM have been studied extensively [20], albeit, with a simplified Hamiltonian, giving rise to extremely low barrier and narrow coexistence region. The recent identification of IBM Hamiltonians without such restrictions [21] enables, for the first time, a comprehensive analysis across a generic first-order QPT.

For the Hamiltonian of Eq. (2), the above procedure yields the following classical potential

$$V^I(\rho)/h_2 = \beta_0^2 \beta^2 - \rho \beta_0^2 \sqrt{2 - \beta^2} \beta^3 \Gamma + \frac{1}{2} (1 - \beta_0^2) \beta^4, \quad (3a)$$

$$V^{II}(\xi)/h_2 = \beta_0^2 [1 - \xi(1 + \beta_0^2)] \beta^2 - \beta_0 \sqrt{2 - \beta^2} \beta^3 \Gamma + \frac{1}{4} [2(1 - \beta_0^2) + \xi(1 + \beta_0^2)^2] \beta^4 + \xi \beta_0^4, \quad (3b)$$

where  $\Gamma \equiv \cos 3\gamma$ . The variables  $\beta \in [0, \sqrt{2}]$ ,  $\gamma \in [0, 2\pi)$  can be interpreted as polar coordinates in an abstract plane parametrized by Cartesian coordinates  $x = \beta \cos \gamma$

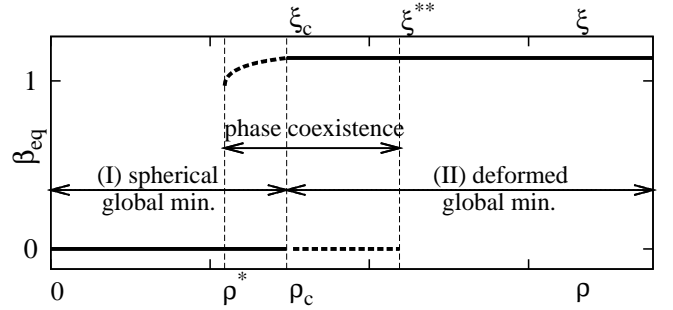


FIG. 1: Behavior of the order parameter,  $\beta_{\text{eq}}$ , as a function of the control parameters ( $\rho, \xi$ ) of the Hamiltonian (2). Here  $\rho^*$ , ( $\rho_c, \xi_c$ ),  $\xi^{**}$ , are the spinodal, critical and anti-spinodal points, respectively, given by  $\rho^* = \frac{1}{\sqrt{6}}[-(r^2 - 4r + 1) + (r + 1)\sqrt{(r + 1)(r - 1/3)}]^{1/2}$ , ( $\rho_c = \beta_0^{-1}$ ,  $\xi_c = 0$ ),  $\xi^{**} = (1 + \beta_0^2)^{-1}$ , with  $r \equiv \beta_0^{-2}$ . The deformation at the global (local) minimum of the Landau potential (3) is marked by solid (dashed) lines.  $\beta_{\text{eq}} = 0$  [ $\beta_{\text{eq}} = \sqrt{2}\beta_0(1 + \beta_0^2)^{-1/2}$ ] on the spherical [deformed] side, with values shown correspond to  $\beta_0 = 1.35$ .

and  $y = \beta \sin \gamma$ . The potential  $V^I(\rho)$  [ $V^{II}(\xi)$ ] has a global spherical [deformed] minimum with, respectively,  $\beta_{\text{eq}} = 0$  [ $\beta_{\text{eq}} > 0, \gamma_{\text{eq}} = 0$ ]. At the spinodal point ( $\rho^*$ ),  $V^I(\rho)$  develops an additional local deformed minimum, and the two minima become degenerate at the critical point  $\rho_c$  (or  $\xi_c$ ). The spherical minimum turns local in  $V^{II}(\xi)$  for  $\xi > \xi_c$  and disappears at the anti-spinodal point ( $\xi^{**}$ ). The order parameter  $\beta_{\text{eq}}$ , shown in Fig. 1, is a double-valued function in the coexistence region (in-between  $\rho^*$  and  $\xi^{**}$ ) and a step-function outside it. The potentials  $V(\beta, \gamma = 0) = V(x, y = 0)$  for several values of  $\xi, \rho$ , are shown at the bottom rows of Figs. 2-3 [panels (a)-(e)]. The height of the barrier at the critical point is  $V_b = h_2 [1 - (1 + \beta_0^2)^{1/2}]^2 / 2$ . Henceforth, we set  $\beta_0 = 1.35$  for which  $V_b/h_2 = 0.231$  (compared to  $V_b/h_2 = 0.0018$  in previous works [20]).

The classical dynamics of  $L = 0$  vibrations, governed by  $\hat{H}_{\text{int}}$  (2), can be depicted conveniently via Poincaré sections [22]. These are shown for selected energies below the domain boundary  $E_{\text{lim}} = V(\beta = \sqrt{2}, \gamma)$ , and control parameters,  $\rho \leq \rho_c$  in Fig. 2 and  $\xi > \xi_c$  in Fig. 3. For  $\rho = 0$ , the system is integrable, with  $V^I(\rho = 0) \propto \beta_0^2 \beta^2 + \frac{1}{2}(1 - \beta_0^2) \beta^4$ . The sections for  $\rho = 0.03$  in Fig. 1, show the phase space portrait typical of an anharmonic (quartic) oscillator (AO) with two major regular islands, weakly perturbed by the small  $\rho \cos 3\gamma$  term. For small  $\beta$ ,  $V^I(\rho) \approx \beta^2 - \rho \sqrt{2} \beta^3 \cos 3\gamma$ . The derived phase-space portrait, shown for  $\rho = 0.2$  in Fig. 2, is similar to the Hénon-Heiles system (HH) [23] with regularity at low energy [panels (b<sub>1</sub>)-(b<sub>2</sub>)] and marked onset of chaos at higher energies [panels (b<sub>3</sub>)-(b<sub>5</sub>)]. The chaotic component of the dynamics increases with  $\rho$  and maximizes at the spinodal point  $\rho^* = 0.546$ . The dynamics changes profoundly in the coexistence region, shown for  $\rho = 0.65, 0.741$  in

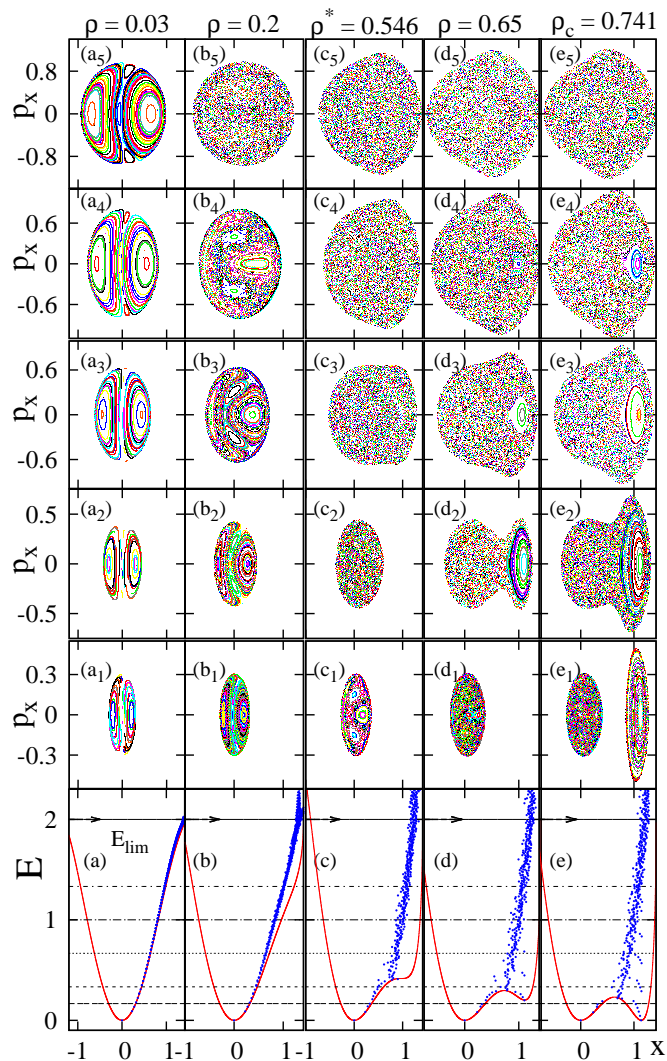


FIG. 2: (Color online). Poincaré sections (upper five rows) depicting the classical dynamics of  $\hat{H}_{\text{int}}^I(\rho)$  (2a) with  $h_2 = 1$ ,  $\beta_0 = 1.35$ , for several values of  $\rho \leq \rho_c$ . The bottom row displays the corresponding classical potentials  $V^{(I)}(\rho)$  (3a). The five energies, below  $E_{\text{lim}} = 2h_2$ , at which the sections were calculated consecutively, are indicated by horizontal dashed lines. The Peres lattices  $\{x_i, E_i\}$ , portraying the quantum dynamics for eigenstates  $|i\rangle$  of  $\hat{H}_{\text{int}}^I(\rho)$  with  $L=0$  and  $N=50$ , are overlaid on the classical potentials  $V(x, y=0)$ .

Fig. 2 and  $\xi=0.05$  in Fig. 3. As the local deformed minimum develops, robustly regular dynamics attached to it appears. The trajectories form a single island and remain regular at energies well above the barrier height  $V_b$ , clearly separated from the surrounding chaotic environment. As  $\xi$  increases, the spherical minimum becomes shallower, the HH-like dynamics diminishes and disappears at the anti-spinodal point  $\xi^{**} = 0.354$ . Regular motion prevails for  $\xi > \xi^{**}$ , where the section landscape changes from a single to several regular islands. The dynamics is sensitive to local degeneracies of normal-modes,

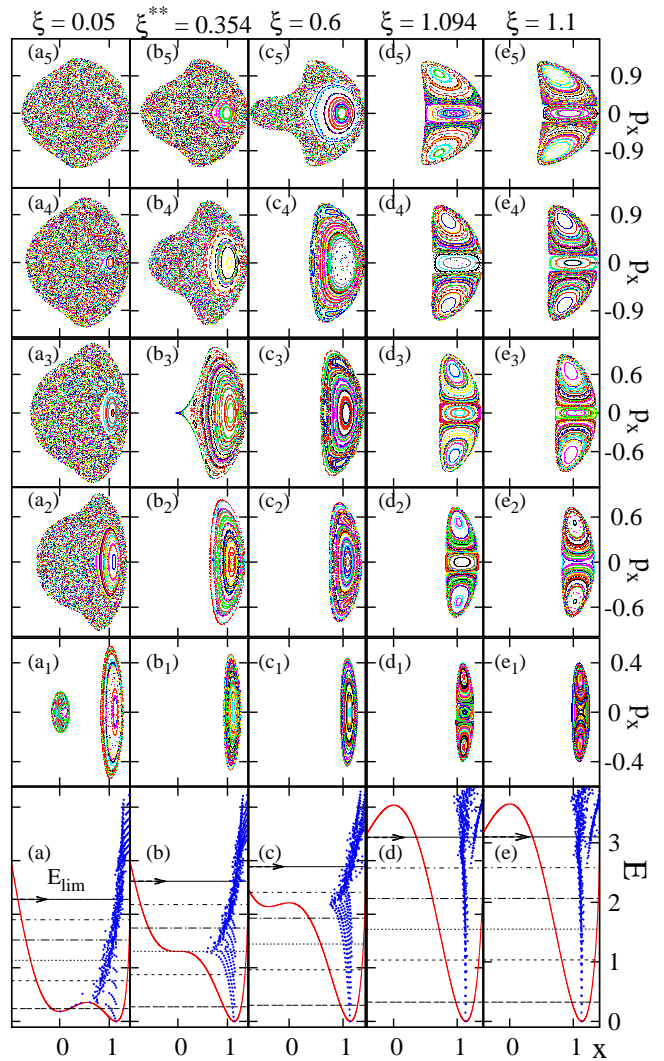


FIG. 3: (Color online). Same as in Fig. 2 but for the intrinsic Hamiltonian  $\hat{H}_{\text{int}}^{II}(\xi)$  (2b) and classical potential  $V^{(II)}(\xi)$  (3b), with  $\xi > \xi_c$  and  $E_{\text{lim}} = h_2(2 + \xi)$ . Notice in the Peres lattices  $\{x_i, E_i\}$  at the bottom row, the sequences of regular states in the deformed region  $x \approx 1$  [also observed in Figs. 2(d)–2(e)]. The lowest sequence consists of  $(N = 50, L = 0)$  bandhead states of the ground  $g(K = 0)$  and  $\beta^n(K = 0)$  bands. Regular sequences at higher energy correspond to  $\beta^n\gamma^2(K = 0)$ ,  $\beta^n\gamma^4(K = 0)$  bands, etc.

as can be seen by comparing Fig. 3(d<sub>1</sub>) for  $\xi=1.094$ , corresponding to  $\epsilon_\beta = \epsilon_\gamma$ , with Fig. 3(e<sub>1</sub>) for  $\xi=1.1$ .

The quantum manifestations of the above rich classical dynamics can be studied via Peres lattices  $\{x_i, E_i\}$  [24]. Here  $E_i$  are the energies of eigenstates  $|i\rangle$  of the Hamiltonian and  $x_i \equiv \sqrt{2\langle i|\hat{n}_d|i\rangle/N}$ . The lattices can distinguish regular from irregular states by means of ordered patterns and disordered meshes of points, respectively [24, 25]. The particular choice of  $x_i$  can associate the states with a given region in phase space through the classical-quantum correspondence  $\beta = x \leftrightarrow x_i$ , ob-

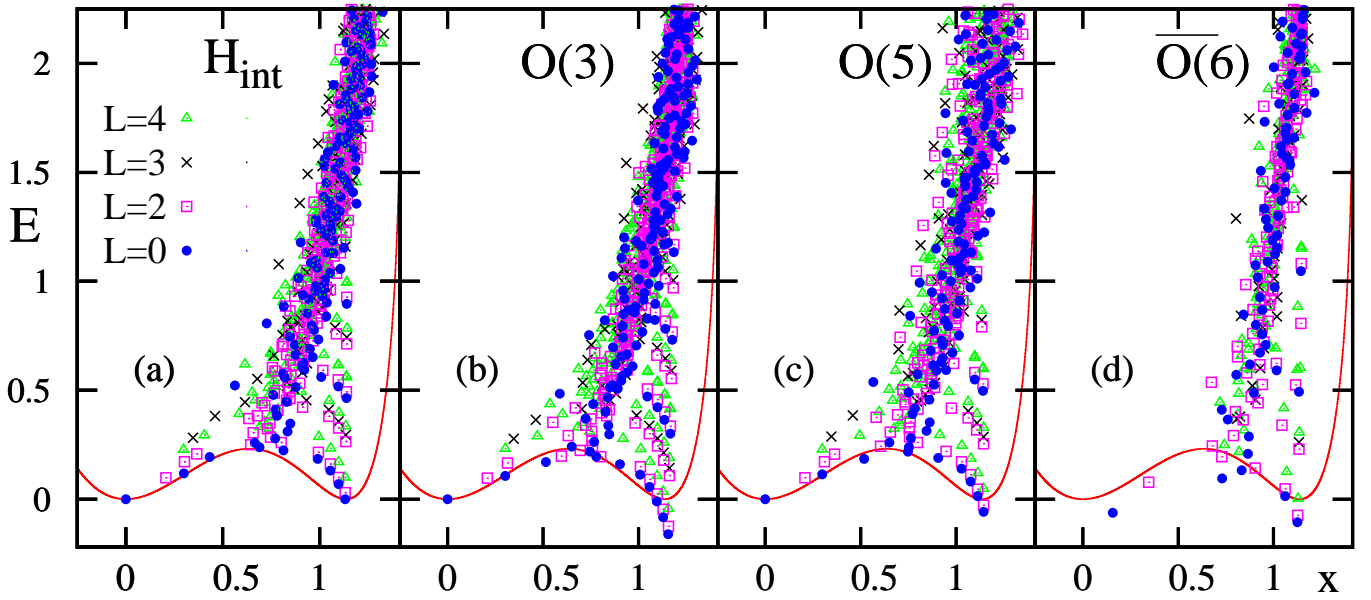


FIG. 4: (Color online). Peres lattices  $\{x_i, E_i\}$  for  $N = 50$ ,  $L = 0, 2, 3, 4$  eigenstates of  $\hat{H}_{\text{int}}^I(\rho = \rho_c)$  (2a), with  $h_2 = 1$ ,  $\beta_0 = 1.35$  [panel (a)] and additional collective terms, Eq. (4), with  $c_i = 1$ , involving  $O(3)$ ,  $O(5)$  and  $\overline{O(6)}$  rotations [panels (b), (c), and (d)]. To enhance visibility, a small energy shift  $\Delta E_L = 0.005L(L + 1)$  is added. The classical potential shown, is the same in all cases. Notice in panels (a)-(b)-(c), the well-developed rotational bands ( $K=0$ ,  $L=0, 2, 4$ ) and ( $K=2$ ,  $L=2, 3, 4$ ) formed by the regular states in the deformed phase, which are distorted in panel (d).

tained by comparing with the expectation value of  $\hat{n}_d$  in the static condensate [11]. The Peres lattices for  $L = 0$  eigenstates of  $\hat{H}_{\text{int}}$  (2) with  $N = 80$ , are shown on the bottom rows of Figs. 2-3, overlaid on the classical potentials  $V(x, y = 0)$ . For  $\rho = 0$ , the Hamiltonian (2a) has  $U(5)$  dynamical symmetry with a solvable spectrum  $E_i = 2\hbar_2[\beta_0^2 N - 1 + (1 - \beta_0^2)n_d]n_d$ . For large  $N$  and replacing  $x_i$  by  $\beta$ , the Peres lattice coincides with  $V^I(\rho = 0)$ , a trend seen in Fig. 2(a). Whenever a deformed minimum occurs in the potential, the Peres lattices exhibit regular sequences of states, localized in the region of the deformed well and persisting to energies well above the barrier. They are related to the regular islands in the Poincaré sections and are well separated from the remaining states, which form disordered (chaotic) meshes of points at high energy. The number of such sequences is larger when the potential well is deeper. The regular  $L = 0$  states form bandheads of rotational sequences  $L = 0, 2, 4, \dots$  ( $K = 0$  bands). Additional  $K$ -bands with  $L = K, K + 1, K + 2, \dots$  can also be identified. An example of such regular  $K = 0, 2$  bands for  $\hat{H}_{\text{int}}$  at the critical point, is shown in Fig. 4(a). In the nuclear physics terminology, the lowest  $K = 0$  band refers to the ground band and excited  $K$ -bands correspond to multiple  $\beta$  and  $\gamma$  vibrations about the deformed shape with angular momentum projection  $K$  along the symmetry axis. The states in each band share a common intrinsic structure as indicated by their nearly equal values of  $\langle \hat{n}_d \rangle$ , and a coherent decomposition of their wave functions in the rotor

basis [26]. The occurrence of such a pure ordered band structure amidst a complicated environment, indicates the relevance, for QPTs, of an adiabatic separation of modes [27] and possibly partial symmetries [28], for a subset of states.

So far the discussion involved the intrinsic part of the Hamiltonian (1). The collective part, which does not affect  $V(\beta, \gamma)$  can be transcribed in the form [18]

$$\hat{H}_{\text{col}} = \bar{c}_3[\hat{C}_{O(3)} - 6\hat{n}_d] + \bar{c}_5[\hat{C}_{O(5)} - 4\hat{n}_d] + \bar{c}_6[\hat{C}_{\overline{O(6)}} - 5\hat{N}], \quad (4)$$

where  $\hat{C}_G$  denotes the quadratic Casimir operator of the group  $G$ , as defined in [18] and  $\bar{c}_i \equiv c_i/N(N - 1)$ . The kinetic  $O(3)$ ,  $O(5)$  and  $O(6)$  terms involve collective rotations associated with the Euler angles,  $\gamma$  and  $\beta$  degrees of freedom, respectively. Fig. 4 shows the Peres lattices corresponding to  $L = 0, 2, 3, 4$  eigenstates of  $\hat{H}_{\text{int}}$  at the critical-point, plus added rotational terms one at a time. As seen in Figs. 4(b)-4(c), the  $O(3)$  and  $O(5)$  terms induce an  $L(L + 1)$ -type in-band splitting and preserve the, previously mentioned, ordered  $K$ -bands of  $\hat{H}_{\text{int}}$ , Fig. 4(a). In contrast, the regular band-structure is strongly disrupted by the  $\overline{O(6)}$  term [Fig. 4(d)]. The latter couples the deformed and spherical configurations [21] and mixes strongly the regular and irregular states. Only the  $\overline{O(6)}$  rotations involve the motion in the  $\beta$  variable [18], highlighting the importance, in QPTs, of the coupling of the order parameter fluctuations with soft

modes [29]. These results demonstrate the advantage of using the resolution of the Hamiltonian (1) in studies of QPTs, since a strong  $\overline{O(6)}$  term in the collective part can obscure the simple patterns of the dynamics disclosed by the intrinsic part.

In summary, we have presented a comprehensive analysis of the dynamics across a generic first order QPT between stable spherical and deformed configurations in the IBM framework. The intrinsic part of the Hamiltonian determines the Landau potential, and its classical analysis reveals a change in the system from an AO- and HH-type of dynamics on the spherical side, into a pronounced regular dynamics on the deformed side of the transition. The dynamics inside the coexistence region is robustly regular and confined to the deformed well, in marked separation from the chaotic behavior ascribed to the spherical well. The coexistence of regular and chaotic motion persists in a broad energy range throughout the coexistence region and is absent outside it. This simple pattern manifests itself also in the quantum analysis, disclosing regular rotational bands in the deformed region, which persist to energies well above the barrier and retain their identity amidst a complicated environment. Kinetic terms in the collective part of the Hamiltonian involving rotations in the orientation (Euler angles) and triaxiality ( $\gamma$ ) variables, preserve the ordered band-structure, while collective rotations in the deformation ( $\beta$ ) variable can disrupt it by mixing regular and irregular states.

This work is supported by the Israel Science Foundation.

- 
- [1] J.A. Hertz, Phys. Rev. B **14**, 1165 (1976).  
 [2] R. Gilmore and D.H. Feng, Nucl. Phys. A **301**, 189 (1978); R. Gilmore, J. Math. Phys. **20**, 891 (1979).  
 [3] *Understanding Quantum Phase Transitions*, edited by L. Carr, CRC press (2010).

- [4] C. Emary and T. Brandes, Phys. Rev. Lett. **90**, 044101 (2003); Phys. Rev. E **67**, 066203 (2003).  
 [5] C.A. Marianetti, G. Kotliar and G. Ceder, Nature Mater. **3**, 627 (2004).  
 [6] C. Pfeleiderer, J. Phys.: Condens. Matter **17**, S987 (2005).  
 [7] C. Pfeleiderer, Rev. Mod. Phys. **81**, 1551 (2009).  
 [8] B. Karmakar, V. Pellegrini, A. Pinczuk, L.N. Pfeiffer, and K.W. West, Phys. Rev. Lett. **102**, 036802 (2009)  
 [9] P. Cejnar, J. Jolie and R.F. Casten, Rev. Mod. Phys. **82**, 2155 (2010).  
 [10] A.P. Young, S. Knysh, and V.N. Smelyanskiy, Phys. Rev. Lett. **104**, 020502 (2010).  
 [11] M. Macek and A. Leviatan, Phys. Rev. C, **84**, 041302(R) (2011).  
 [12] L.A. Bunimovich, Chaos, **11**, 802 (2001).  
 [13] B. Dietz, T. Friedrich, M. Miski-Oglu, A. Richter and F. Schäfer, Phys. Rev. E **75**, 035203(R) (2007).  
 [14] F. Iachello and A. Arima, *The Interacting Boson Model* (Cambridge University Press, Cambridge, UK, 1987).  
 [15] A.E.L. Dieperink, O. Scholten and F. Iachello, Phys. Rev. Lett. **44**, 1747 (1980).  
 [16] P. Cejnar and J. Jolie, Prog. Part. Nucl. Phys. **62**, 210 (2009).  
 [17] F. Iachello, Rivista Del Nuovo Cimento **34**, 617 (2011).  
 [18] A. Leviatan, Ann. Phys. (NY) **179**, 201 (1987).  
 [19] R.L. Hatch and S. Levit, Phys. Rev. C **25**, 614 (1982).  
 [20] N. Whelan and Y. Alhassid, Nucl. Phys. A **556**, 42 (1993).  
 [21] A. Leviatan, Phys. Rev. C **74**, 051301(R) (2006).  
 [22] L. E. Reichl, *The Transition to Chaos in Conservative Classical Systems: Quantum Manifestations* (Springer-Verlag, New York, 1992).  
 [23] M. Hénon and C. Heiles, Astron. J. **69**, 73 (1964).  
 [24] A. Peres, Phys. Rev. Lett. **53**, 1711 (1984).  
 [25] P. Stránský, P. Hruška and P. Cejnar, Phys. Rev. E **79**, 066201 (2009).  
 [26] M. Macek and A. Leviatan, in preparation.  
 [27] M. Macek, J. Dobeš, P. Stránský and P. Cejnar, Phys. Rev. Lett. **105**, 072503 (2010).  
 [28] A. Leviatan, Phys. Rev. Lett. **98**, 242502 (2007).  
 [29] D. Belitz, T.R. Kirkpatrick and T. Vojta, Rev. Mod. Phys. **77**, 579 (2005).